ISSN 1392-1207. MECHANIKA. Vol. 31, No. 3, 2025: 230–236

Numerical Investigation of Yield Stress and Damping Force for a Modeled Damper Using Different MR Fluids

Vinod CHAUHAN, Ashwani KUMAR, Radhey SHAM

Department of Mechanical Engineering, Chandigarh College of Engineering & Technology (Degree Wing), Chandigarh, India, 160019, E-mails: vinodchauhan@ccet.ac.in, ashwanikumar@ccet.ac.in, radheysham@ccet.ac.in

https://doi.org/10.5755/j02.mech.37031

1. Introduction

The researchers aim to explore vibration control techniques in automotive setups, industrial equipment, civil structures, etc., which vibrate abruptly. The magnetorheological (MR) dampers, which act as a means of vibration control are used to mitigate the generated vibrations. Magnetorheology is formulated to understand how an applied magnetic field manipulates the fluid's rheology. Jacob Rabinow prepared/developed the MR fluid in 1948 at the US National Standards Bureau [1]. A MR damper has been designed and evaluated for its damping behavior, i.e., damping force experimentally as well as using the FEA approach. The damping force obtained through both approaches matched well over a wider range of supplied currents. [2]. The MR damper is most practiced in motor vehicle suspensions; however, its use has lately been escalated to other significant structures such as bridges, buildings, landing gear, prosthetic limbs, washing machines, etc. [3-6]. Acharya et al. [7] developed the MR fluid having optimal Fe particle loading and Fe particle size for a mono-tube MR damper. The MR fluid samples, combining the various particle loadings and Fe particle sizes, were tested to obtain the flow profiles at off-state as well as on-state conditions. Magnetostatic analysis has been practiced to estimate the induced magnetic field strength in the MR fluid gap at varying currents. The optimal dynamic yield stress and optimal damping force were determined for the modeled damper. Nanthakumar and Jancirani [8] investigated the impact of various design attributes on the yield stress of a modeled MR damper. The magnetic strength induced in the fluid gap was estimated using the COMSOL Multiphysics platform. A quadratic expression has been formulated for the response parameter i.e., yield stress using the full factorial design of the experiments approach. Purandare et al. [9] determined the induced field in the MR damper using the COMSOL Multiphysics method and validated the results with magnetic circuit theory. A deviation of 4.8% was observed between the COMSOL and the analytical value of magnetic flux developed in the fluid gap for an input current of 1 ampere. Li and Yang [10] established a numerical model to estimate the damping force of a modeled MR damper having non-magnetized piston passages. In the modeled damper, the pressure drops resulting from the MR effect, viscous loss, and the minor loss at the passage inlet & outlet have been taken into account. The errors obtained for the evaluated damping force that includes both viscous loss and minor loss were found to be much less in comparison with the results that include viscous loss only. It exhibits that the pressure drops resulting from the minor losses are of much significance and can't be neglected. The numerical model considering both viscous as well as minor losses is highly effective in estimating the stroke load of the MR damper in comparison with the model in which minor losses are not included.

Kemerli and Engin [11] designed the monotube type mixed-mode MR damper by applying the FEA approach along with the computational fluid dynamics (CFD) technique. The numerically obtained force-velocity and force-displacement results for different input currents matched well with their experimental results. The CFD outputs are substantial in estimating the realistic attributes of the non-Newtonian fluid flowing in the MR damper. Badri et al. [12] conducted a CFD analysis for a damper in a car rear suspension system using MRF-132DG. A 70% rise in viscosity was observed when the current varied from 0A - 5A. The rebound and compression steady pressure values determined from contour illustrations were used to obtain the value of the generated damping force. The damping force improved exponentially with a rise in viscosity. Elsaady et al. [13] investigated the impact of air bubbles present inside the MR (AMT-Smartec+) fluid on the performance of a designed damper. The off-state viscosity's higher value of the used fluid results in retaining the air bubbles. The results indicated a reasonable decline in the calculated value of the damping force. Hu et al. [14] established the electromagnetic field model, mechanical model, structural stress field, and flow field model for the MR damper. The stress distribution, static & dynamic field attributes, and dynamical performance of the designed MR damper have been determined. The damper exhibited an appropriate damping force value along with a wider adjustable damping range. An error of 5.5% and 9.9% has been observed between the experimental and simulation output for the generated damping force and adaptable damping coefficient respectively. Marathe et al. [15] designed a lower-cost MR damper, with a focus on optimizing geometric attributes of the annular valve using the Taguchi technique. A higher damping force and lower resulting force transmissibility have been observed for the developed damper in comparison with the passive damper, which improved the comfort and handling for vehicles.

Aralikatti et al. [16] evaluated the influence of base-oil viscosity and CI particle fraction on the damping range and largest yield stress of a little-stroke MR damper fitted on a lathe machine to control the tool vibrations. An improvement of 28.66% in the level of tool vibration and 68.18% in cutting force amplitude has been noticed. A significant improvement in surface roughness (value declines from 4.8 μm to 1.6 μm) has also been noticed. Abdalaziz et al. [17] designed a varying stiffness and varying damping capacity MR damper having a spherical-radial bypass valve. The designed damper exhibited a damping force of 7800 N

and a dynamic range of 4.5. Liang et al. [18] introduced a simulation model operating on a gas counterbalance to a single-rod MR damper for characterizing its performance precisely. The impact of the compensating mechanism on the damper's performance under varying excitation currents, speeds etc. has been investigated. The experimental and simulation results were found to be in good agreement with one another. Delijani et al. [19] proposed a novel model combining the features of a parametric model and a neural network model. In the suggested model, the parametric features employ an algebraic model accompanied by hyperbolic tangent-type hysteresis, while a set of multilayered perceptron neural networks is utilized to establish the model attributes under varying excitation settings. The developed model exhibited a more accurate predicted damping force and indicated greater strength and improved consistency under varying excitations in comparison with a conventional model. Kumar et al. [20] developed a novel machine learning-based black box model that precisely forecasts the complex damping characteristics exhibited by MR dampers, thereby improving both ride comfort and vehicle safety. A machine learning technique integrated with real feedback control was used, thereby securing the model's reliability and accuracy. Fu et al. [21] analyzed the damping behavior of MR mounts by establishing the fluid motion equation in the channel based on a parallel plate model. The effect of magnetic core depth, height of inertial channel, etc. on the magnetic flux density along with the damping force has been investigated. Kumbhar et al. [22] developed a MR dynamic vibration absorber mechanism using MR fluid to regulate vibrations generated in a quarter-car suspension system. The mechanism has been validated using experimental and numerical approaches.

Kim et al. [23] investigated damping capability of the MR damper having an additional flow passage. An optimal model using fluid dynamic relations was designed and evaluated by electromagnetic analysis using ANSYS Maxwell software. The Amesim software has been used for carrying out vibrational analysis utilizing a sinusoidal road surface model at different frequency values. Bajkowski et al. [24] evaluated a novel synthesized MR fluid in a translation vibrational damper having a varying excitation frequency range. The damper's response of compressible fluids exhibited a significant variation from that noticed incase of non-compressible fluids. On activation, the MR fluid's motion resistance gets improved, thereby enhancing the damper's flexible response. Jin et al. [25] proposed a MR fluid-based damper model for use in motor vehicle engine mountings. The precise design of the magnetic circuit has been validated using static field simulation. A genetic algorithm for the proposed model has been utilized to recognize its various parameters. The proposed MR damper efficiently minimizes the vibrations passed from the engine to body, thereby enhancing the damper's damping performance. Silva et al. [26] proposed an innovative hybrid optimal methodology that integrates a differential evolution algorithm together with a native approach adopting Nelder-Mead simplex searchable technique. It incorporates an empirical design to govern the excited frequency, input current, as well as piston displacement.

2. Magnetorheological Damper Design

The MR damper design relies on its load-carrying capacity, availability of material, and size constraints.

2.1. Basic geometry

The MR fluid passage in MR dampers is normally held in the range of 0.5 mm - 2 mm to generate an effective magnetorheological effect. The magnetic flux navigates right through the outer pole and arrives at inner pole within the MR fluid passage, building a closed magnetized loop. The schematic of the modeled magnetorheological damper is presented in Fig. 1 [27]. The materials assigned to the piston and cylinder are low-carbon steel (steel 1008), while the coil (size - 26 gauge) is made up of copper. Nitrile Butadiene Rubber (NBR) seals are provided to prevent any leakage in the modeled damper. The in-house synthesized optimal MR sample contains silicon oil as carrier fluid, carbonyl iron particle (6 μm average particle size), iron particle proportion as 24% (by volume), and ethylene glycol mono-stearate (1% by volume) as an additive.

2.2. Geometrical parameters

A detailed magnetic circuit for the modeled MR damper is presented in Fig. 2 [27]. A 2-dimensional axis-symmetric MR damper model has been designed to perform the Finite Element Analysis (FEA).

The geometrical parameters (outer piston radius, inner piston radius, piston head length, pole length, cylinder thickness, fluid gap, coil width) for the modeled MR damper are demonstrated in Table 1.

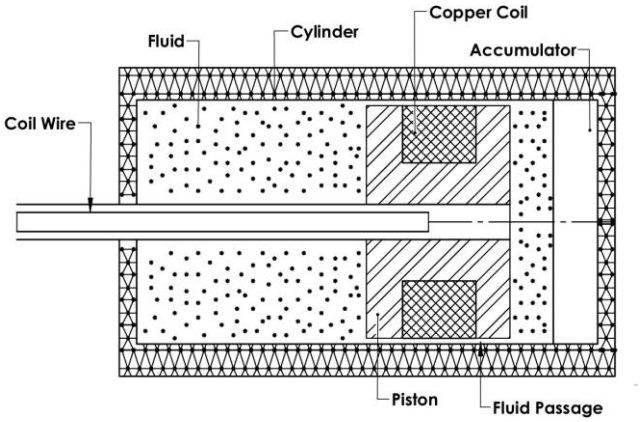

Fig. 1 Schematic of MR damper

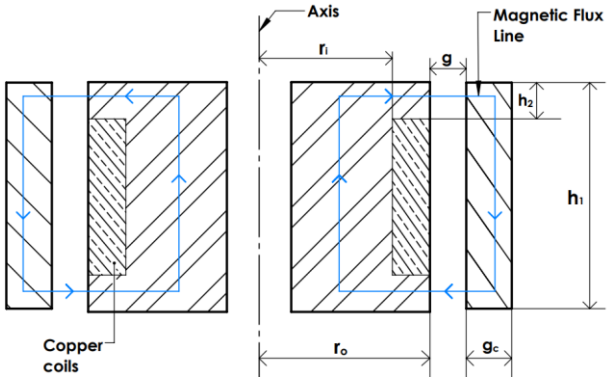

Fig. 2 Magnetic circuit for modeled MR damper

Table 1

MR damper dimensions in mm

Outer piston radius (r_o)	24.10
Inner piston radius (r_i)	12.30
Pole length (h_2)	12.00
Cylinder thickness (g_c)	5.00
Piston head length (h_1)	45.00
Coil width (b)	11.80
Fluid gap (g)	0.90

3. Determination of Magnetic Field Intensity Using FEA

The magnetic field Intensity (H) may be obtained by performing a magnetostatic analysis on the modeled MR damper. An axisymmetric analysis of the geometrical MR damper is sufficient for solving the problem instead of performing the analysis of the complete geometry. ANSYS Maxwell v.16 software, utilized for this purpose, is very much capable of computing the Maxwell equations and assessing the values of the magnetic field at different points inside the fluid gap. The magnetic field intensity plots and magnetic flux lines plots at 0.8 ampere for the MR damper filled with in-house synthesized optimal MR fluid sample are presented in Fig. 3 and 4, respectively.

The computed values of magnetic field intensity at different input currents (0.1 – 0.8 A) for various MR fluids have been presented in Fig. 5.

4. Results and Discussion

An important stage in designing of MR damper is the determination of deviation in the MR fluid yield stress with change in the magnetic field. After computing the yield stress, the total damping force has been obtained using Eqs. (7)-(11).

4.1. Computation of yield stress

After computing the magnetic field intensity by performing magnetostatic analysis, the equations representing the yield stress relation with the intensity of the magnetic field (τ_y-H equations) for various MR fluids are obtained using the least squares technique, rheological plots published in the research, and the manufacturer's datasheet

$$\tau_y = 7\times10^{-7}H^3 - 7.84\times10^{-4}H^2 + \\ +0.2898H - 1.2206, \quad (1)$$

$$\tau_y = 5\times10^{-7}H^3 - 9.03\times10^{-4}H^2 + \\ +0.3893H - 1.182, \quad (2)$$

$$\tau_y = 2\times10^{-7}H^3 - 1.149\times10^{-3}H^2 + \\ +0.5655H + 0.9609, \quad (3)$$

$$\tau_y = 2.38\times10^{-8}H^3 - 5.63\times10^{-4}H^2 + \\ +0.293H - 0.7201, \quad (4)$$

$$\tau_y = 3.7\times10^{-6}H^3 - 2.3\times10^{-3}H^2 + \\ +0.6035H + 0.2158, \quad (5)$$

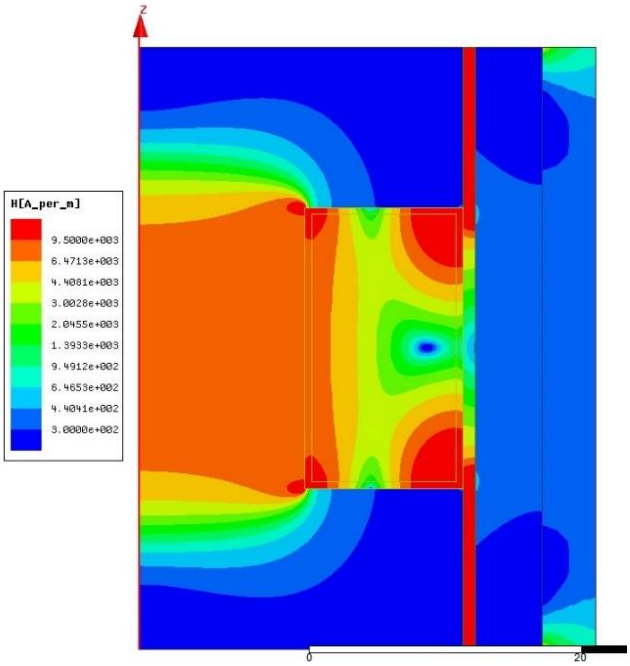

Fig. 3 Magnetic field intensity plot at 0.8 ampere for the MR damper filled with in-house synthesized optimal MR fluid sample

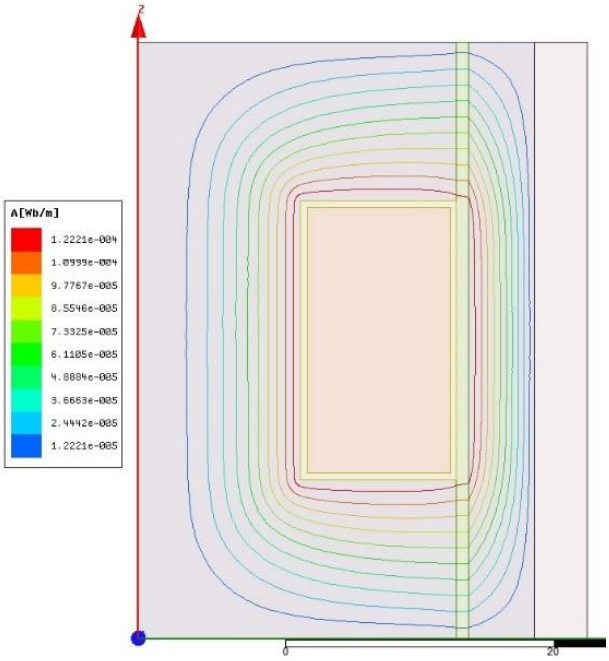

Fig. 4 Magnetic flux line plot at 0.8 amperes for the MR damper filled with in-house synthesized optimal MR fluid sample

$$\tau_y = 4.5\times10^{-6}H^3 - 2.9\times10^{-3}H^2 + \\ +0.7436H + 0.2066. \quad (6)$$

In the above equations (Eq. (1)-Eq.(6)), H is represented in terms of kA/m and τ_y in terms of kPa. These Eqs. (1-6) represent the τ_y-H relations for MRF-122 EG, MRF-132DG, MRF-140CG, in-house prepared Optimal MR fluid, AMT MAGNAFLO$^+$, and AMT RHEOTEC$^+$. The computed values of yield stress for various MR fluids are presented in Fig. 6. The yield stress is enhanced non-linearly for all fluids used in the present study when the input current

increases from 0.1 - 0.8 A. The computed yield stress is maximum for AMT RHEOTEC$^+$ fluid and lowest for MRF-122EG for all input current values.

Initially, the yield stress improves rapidly, but the increment in yield stress declines with a further increase in the input current. The computed yield stress of the in-house synthesized optimal MR fluid exhibits good agreement with the commercially available MR fluids.

4.2. Computation of shear, viscous and total damping force

The total damping force (F) is composed of shear force (F_τ), viscous force (F_η), and frictional force (F_f) [28]:

$$F = F_\tau + F_\eta + F_f , \tag{7}$$

$$F_\eta = Q\frac{6\eta h_1 A_p}{\pi R_{avg} g^3} , \tag{8}$$

$$F_\tau = 2c\frac{h_2}{g} A_p \tau_y \, sgn\left(v_p\right) , \tag{9}$$

$$R_{avg} = R_o + g + \frac{g_c}{2} , \tag{10}$$

where η denotes the fluid's plastic viscosity, Q denotes the flow rate, v_p denotes the piston's velocity, A_p denotes the piston head's cross-sectional area, R_{avg} is the fluid gap average radius, τ_y denotes shear yield stress, and c is a constant (value range is 2.07-3.07), regulated by flow velocity profiles. The constant (c) is evaluated as follows:

$$c = 2.07 + \frac{6Q\eta}{6Q\eta + 0.4\pi R_{avg} g^2 \tau_y} . \tag{11}$$

The computed shear damping force, which is the controllable force in the MR dampers, is presented in Fig. 7. AMT RHEOTEC$^+$ fluid exhibits the largest shear damping force, while MRF-122 EG is the one that exhibits the lowest value of it. It is the shear damping force that varies on varying the input current, while the viscous force remains unchanged. The viscous damping force in case of various MR fluids has been presented in Fig. 8.

The MR fluid must possess a lower viscous force to attain a higher dynamic range. The results exhibit that the MRF-140CG owns the largest viscous damping force (204.83 N) while MRF-122EG owns the lowest viscous damping force (30.72 N) for the modeled damper. Hence, from a viscous damping force point of view, MRF-122EG fluid may be considered better in comparison with other MR fluids used in the current study.

The total damping force generated by various MR fluids has been presented in Fig. 9. For the MRF-122EG fluid the total damping force for the modeled damper increased from 60.72 N to 1571.86 N when the current varied from 0 A to 0.8 A. Incase of in-house prepared optimal MR fluid, the computed value of total damping force rises from 70.23 N to 1770.02 N for similar variation in the input current. The magnitude of total damping force is enhanced from 111.93 N to 2112 N, 234.83 N to 2440.64 N, 101.69 N to

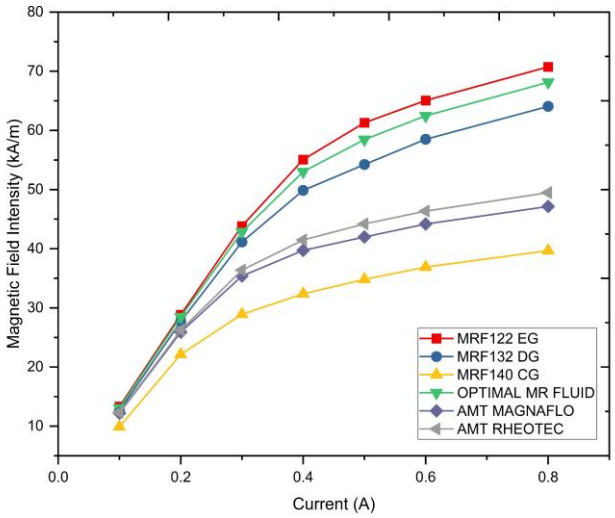

Fig. 5 Magnetic field intensity at different input currents for various MR fluids

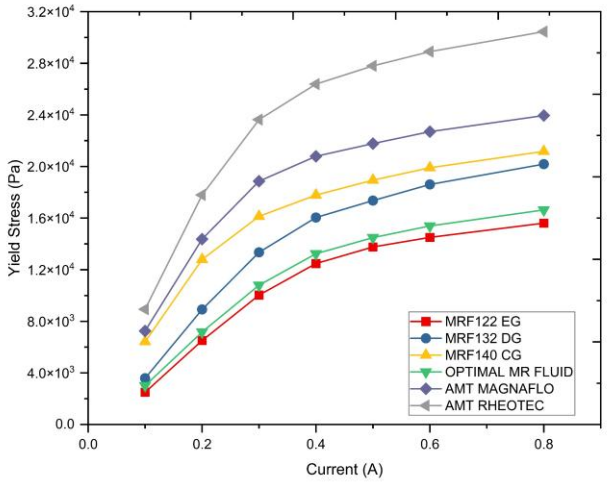

Fig. 6 Yield Stress at different input currents for various MR fluids

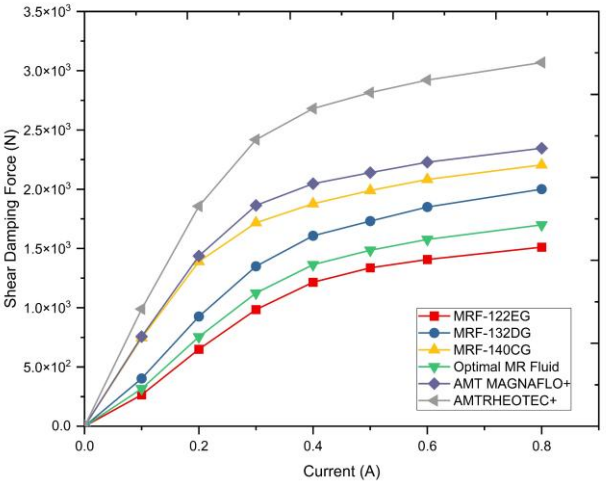

Fig. 7 Shear Damping Force at different input currents for various MR fluids

2447.89 N, 205.57 N to 3274.34 N for MRF-132 DG, MRF-140CG, AMT MAGNAFLO$^+$, AMT RHEOTEC$^+$ fluid, respectively for similar variation in the input current.

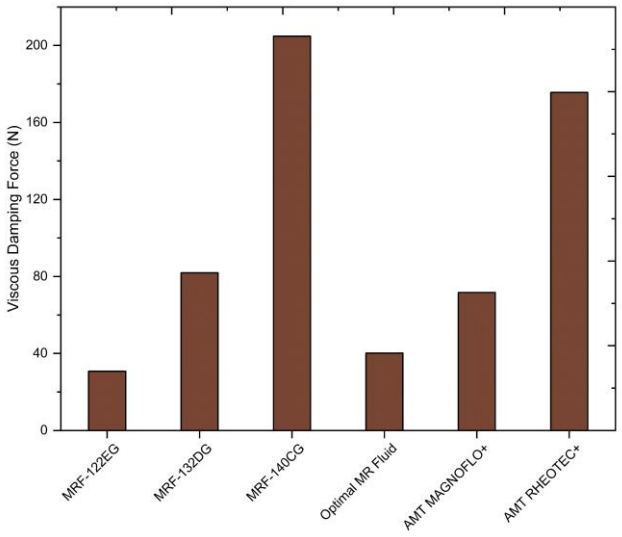

Fig. 8 Viscous damping force for various MR fluids

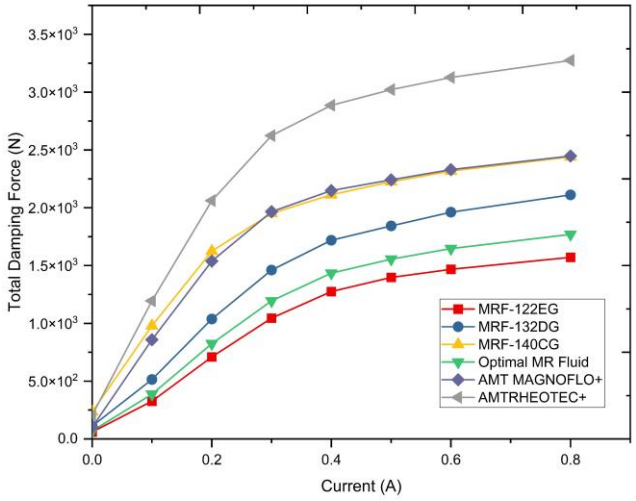

Fig. 9 Total Damping Force at different input currents for various MR fluids

5. Conclusions

The present study investigates the impact of various MR fluids on yield stress as well as the damping capability (damping force) of a modeled MR damper. The magnetic field intensity at varying currents has been determined by performing magnetostatic analysis in ANSYS Maxwell v.16 software. In conformity with the estimated results, the conclusions depicted are given as:

- All the used MR fluids exhibit an improvement in yield stress and damping force with a rise in input current.
- Initially (at lower values of input current), the rise in yield stress is large, but at higher values of current, this rise in yield stress is much less as depicted by the slope of the curve.
- AMT-RHEOTEC^{+} fluid exhibits the highest values of yield stress, while MRF-122 EG fluid depicts the lowest yield stress for all values of input currents.
- MRF-122 EG fluid exhibits the lowest viscous damping force, while MRF-140CG exhibits the highest viscous damping force.
- The total damping force is largest for AMT-RHEOTEC^{+} fluid, while it is lowest for MRF-122 EG fluid at all values of input currents. So, the best MR fluid for the damper is AMT-RHEOTEC fluid. However, the in-house developed optimal MR fluid also exhibited sufficient damping force, which is in good agreement with the commercially available MR fluids.

References

1. **Rabinow, J.** 1948. The magnetic fluid clutch, Electrical Engineering 67(12): 1167– 1167. https://doi.org/10.1109/EE.1948.6444497.
2. **Mangal, S. K.; Kumar, A.** 2014. Experimental and Numerical Studies of Magnetorheological (MR) Damper, Chinese Journal of Engineering: 915694. https://doi.org/10.1155/2014/915694.
3. **Nguyen, Q.; Choi, S.; Woo, J.** 2013. Optimal design of magnetorheological fluid-based dampers for front-loaded washing machines, Proceedings of the Institution of Mechanical Engineers, Part C: Journal of Mechanical Engineering Science 228(2): 294-306. https://doi.org/10.1177/0954406213485908.
4. **Oh, J. S.; Shin, Y. J.; Koo, H. W.; Kim, H. C.; Park, J.; Choi, S. B.** 2016. Vibration control of a semi-active railway vehicle suspension with magneto-rheological dampers, Advances in Mechanical Engineering 8(4): 1687814016643638. https://doi.org/10.1177/1687814016643638.
5. **Xie, J.; Liu, C.; Cai, D.** 2020. Analysis and Experimental Study on Rheological Performances of Magnetorheological Fluids, Mechanika 26(1): 31-34. https://doi.org/10.5755/j01.mech.26.1.25244.
6. **Dakshnamoorthy E.; Arjunan S.; Radhakrishnan A.; Gopal A.** 2023. Study on the Influence of Synthesized Nano Ferrite Powder and Micron Ferrite Powder on Damping of a Single Degree of Freedom System, Mechanika 29(4): 334-339. https://doi.org/10.5755/j02.mech.32055.
7. **Acharya, S.; Saini, T. R. S.; Kumar, H.** 2019. Determination of optimal magnetorheological fluid particle loading and size for shear mode monotube damper, Journal of the Brazilian Society of Mechanical Sciences and Engineering 41: 392. https://doi.org/10.1007/s40430-019-1895-4.
8. **Nanthakumar, A. J. D.; Jancirani, J.** 2019. Design optimization of magnetorheological damper geometry using response surface method for achieving maximum yield stress, Journal of Mechanical Science and Technology 33: 4319-4329. https://doi.org/10.1007/s12206-019-0828-6.
9. **Purandare, S.; Zambare, H.; Razban, A.** 2019. Analysis of magnetic flux in magneto-rheological damper, Journal of Physics Communications 3(7): 075012. https://doi.org/10.1088/2399-6528/ab33d7.
10. **Li, G.; Yang, Z. B.** 2020. Modelling and Analysis of a Magnetorheological Damper with Nonmagnetized Passages in Piston and Minor Losses, Shock and Vibration 2020: 2052140. https://doi.org/10.1155/2020/2052140.
11. **Kemerli, M.; Engin, T.** 2021. Numerical analysis of a monotube mixed mode magnetorheological damper by

using a new rheological approach in CFD, Rheologica Acta, 60: 77-95.
https://doi.org/10.1007/s00397-020-01252-2.

12. **Badri, Y.; Syam, T.; Sassi, S.; Hussein, M.; Renno, J.; Ghani, S.** 2021. Investigating the characteristics of a magnetorheological fluid damper through CFD modeling, Materials Research Express 8(5): 055701.
https://doi.org/10.1088/2053-1591/abfcf6.
13. **Elsaady, W.; Oyadiji, S. O.; Nasser, A.** 2020. Study of failure symptoms of a single-tube MR damper using an FEA-CFD approach, Journal of Intelligent Material Systems and Structures 32(13): 1391-1419.
https://doi.org/10.1177/1045389X20969837.
14. **Hu, G.; Wu, L.; Deng, Y.; Yu, L.; Luo, B.** 2021. Damping Performance Analysis of Magnetorheological Damper Based on Multiphysics Coupling, Actuators 10(8): 176.
https://doi.org/10.3390/act10080176.
15. **Marathe, A. P.; Khot, S. M.; Nagler, J.** 2022. Development of Low-Cost Optimal Magneto-rheological Damper for Automotive Application, Journal of Vibration Engineering & Technologies 10(5): 1831-1850.
https://doi.org/10.1007/s42417-022-00486-z.
16. **Aralikatti, S. S.; Puneet, N. P.; Kumar, H.** 2023. Determining the optimal composition of magnetorheological fluid for a short-stroke magnetorheological damper, Sādhanā 48: 120.
https://doi.org/10.1007/s12046-023-02195-z.
17. **Abdalaziz, M.; Vatandoost, H.; Sedaghati, R.; Rakheja S.** 2023. Design and experimental characterization of a bypass magnetorheological damper featuring variable stiffness and damping, Smart Materials and Structures 32(3): 035011.
https://doi.org/10.1088/1361-665X/acb474.
18. **Liang, H.; Li, J.; Wang, Y.; Liu, M.; Fu, J.; Luo, L.; Yu, M.** 2023. Multi-Physics Simulation and Experimental Verification of Magnetorheological Damper with Additional Stiffness, Actuators 12(6): 251.
https://doi.org/10.3390/act12060251.
19. **Delijani, Y. M.; Cheng, S.; Gherib F.** 2023. Sequential neural network model for the identification of magnetorheological damper parameters, Smart Materials and Structures 33(1): 015002.
https://doi.org/10.1088/1361-665X/ad0f36.
20. **Kumar, K. B.; Babu, K. R. R.; Unnikrishnan, R.; Sangeetha, U.** 2023. Dynamic Behaviour Modelling of Magneto-Rheological Fluid Damper Using Machine Learning, Indian Journal of Science and Technology 16(45): 4233-4243.
https://doi.org/10.17485/IJST/v16i45.1669.
21. **Fu, J.; Huang, C.; Shu, R.; Li, X. Q.; Chen, M.; Chen, Z.; Chen, B.** 2023. Multi-Objective Optimization of Magnetorheological Mount Considering Optimal Damping Force and Maximum Adjustable Coefficient, Machines 11(1): 60.
https://doi.org/10.3390/machines11010060.
22. **Kumbhar, M. B.; Desavale, R. G.; Jagadeesha, T.** 2024. Experimentation and Damping Performance Analysis of a MR Damper for Resonance Control in a Quarter Car Suspension System, Journal of Vibration Engineering & Technologies 12: 5973-5983.
https://doi.org/10.1007/s42417-023-01230-x.
23. **Kim, M.; Yoo, S.; Yoon, D.; Jin, C.; Won, S.; Lee, J.** 2024. Numerical Analysis of the Vehicle Damping Performance of a Magnetorheological Damper with an Additional Flow Energy Path, Applied Sciences 14(22): 10575.
https://doi.org/10.3390/app142210575.
24. **Bajkowski, J. M.; Bajer, C. I.; Dyniewicz, B.; Bajkowski, J.; Leonowicz, M.** 2024. Performance of a vibration damper using a new compressible magnetorheological fluid with microspheres, Smart Materials and Structures 34: 015041.
https://doi.org/10.1088/1361-665X/ad9cd7.
25. **Jin, Z.; Yang, F.; Rui, X.; Jiang, M.; Wang, J.** 2024. Design, Modeling, and Vibration Control of a Damper Based on Magnetorheological Fluid and Elastomer, Actuators 13(7): 241.
https://doi.org/10.3390/act13070241.
26. **Da Silva, D. M. D.; Avila, S. M.; de Morais, M. V. G.; Cavallini A. A.** 2024. Comparing optimization algorithms for Parameter Identification of Sigmoid Model for MR damper, Journal of the Brazilian Society of Mechanical Sciences and Engineering 46: 134.
https://doi.org/10.1007/s40430-024-04698-0.
27. **Chauhan, V.; Kumar, A.; Sham, R.** 2024. Design of Magnetorheological Fluid Damper with Optimal Damping Force, International Journal of Mechanical Engineering and Robotics Research 13(1): 105-112.
https://doi.org/10.18178/ijmerr.13.1.105-112.
28. **Parlak Z.; Engin T.; Şahin İ.** 2013. Optimal Magnetorheological Damper Configuration Using the Taguchi Experimental Design Method, ASME Journal of Mechanical Design 135(8): 081008.
https://doi.org/10.1115/1.4024719.

V. Chauhan, A. Kumar, R. Sham

NUMERICAL INVESTIGATION OF YIELD STRESS AND DAMPING FORCE FOR A MODELED DAMPER USING DIFFERENT MR FLUIDS

S u m m a r y

This article presents the yield stress, shear damping force, viscous damping force, and total damping force generated in a modeled damper using various magnetorheological (MR) fluids. The values of the generated magnetic field intensity in a modeled damper have been obtained by performing a magnetostatic analysis using ANSYS Maxwell v.16 software. All the used MR fluids exhibit growth in yield stress and damping force on increasing input current. The magnetic field intensity values are fitted into (τ_y - H) quadratic equations, which are developed for all the used MR fluids using the least square technique for computing the yield stress. The estimated yield stress is maximum for AMT RHEOTEC$^+$ fluid and lowest for MRF-122EG for all input current values. The computed yield stress of the in-house prepared optimal MR fluid exhibits good agreement with the commercially available MR fluids. The results exhibit that the MRF-140CG owns the largest viscous damping force, while MRF-122EG owns the lowest viscous damping force for the modeled damper. AMT RHEOTEC$^+$ fluid possesses the largest shear damping force (controllable force) as well as total damping force, while MRF-122 EG is the one that exhibits the lowest value for shear as well as total damping force.

Keywords: MR fluid, MR damper, yield stress, shear damping force, viscous damping force, magnetostatic analysis.

Received April 21, 2024
Accepted June 25, 2025